Nanotechnology Perceptions
ISSN 1660-6795
www.nano-*ntp.com*

Particulate Chip Formation During Variable Machining Of EN 47 Steel

Lokesh Kumar Mehra [1, a], Himanshu [2,b] and Kalyan Chakraborty [3,c*]

[1]Mehanical Engineering Department, N.I.T. Silchar, Assam, India, 788010
[2]Mehanical Engineering Department, N.I.T. Silchar, Assam, India, 788010
[3]Mehanical Engineering Department, N.I.T. Silchar, Assam, India, 788010
[a]lokesh1679797@gmail.com, [b]himanshurewar01@gmail.com,
[c]chakrabortykalyan623@gmail.com*

The present work illustrates the machining behaviour of EN47 spring steel during the variable machining. The tool was a Miranda-brazed carbide tool. The variable machining was for different speeds (400 to 1000 rpm) at constant feed (F= 0.1 mm/rev.) and depth of cut (D = 1 mm). The machining time varied between 5 sec and 15 sec. The smallest particulate chips were for machining at a lower speed (400 rpm) during the machining for 15 seconds. The particulate chips formed due to the extensive strain hardening that occurred at a lower speed. Extensive strain hardening favoured the formation of numerous cracks that resulted in the formation of smaller particulates through catastrophic breakage of the chip. The von Mises stress (VMS) was lowest at this machining condition. At moderate speed (630 rpm), the chip formation occurred through deformation in ductile mode. During the machining for higher speed (1000 rpm), chip formation occurred by the following steps (1) elongated sub-grains formation due to dislocation cell formation, and (2) subdivided elongated sub-grain formation. The present objective is to find out the proper machining method to form smaller metallic particulates (average size less than 2 mm) so as to enable the ball milling process to cause further reduction of particulates very easily at a lesser time. The collection of metallic particulates by machining underscores the novelty of the work.

Keywords: Variable machining, particulate chips, ball milling process.

Introduction

The EN 47 steel is used extensively for aerospace and automobile applications. These steels have excellent ease of extrusion, weldability and corrosion resistance. EN47 steel is known as spring steel. This steel can also be used as high-duty leaf springs and heavy engine valve springs. This steel is usually of medium carbon low alloy steel. The EN 47 spring steel has higher hardness, stiffness, wear resistance and shock absorbing ability. EN 47 steel is considered a difficult-to-machine material [1, 2].

The usual method is to cut steel chips for smaller sizes to produce powder particulates by planetary ball milling operations. However, this process results in needless time wastage. The effort is to search for a proper machining method with proper machining parameters so that

much smaller steel chip particulates form by machining the steel in a lathe. This will cause a saving of time during the ball milling operation to obtain powdered metallic particles.

The machining formed the aluminium-bronze chips. Initial preference was to cut the chips to approximately 10 mm in size. Planetary ball milling resulted in powder particles. Mixing of these particles with vanadium carbide occurred in different proportions with process control agents. Further milling of the mixture was to obtain the powder particles at reduced dimensions. The optimization (DOE) work was to find out the optimal combination of ball milling time, speed and percentage addition of vanadium carbide particles. The experimental milling time ranged between 10 to 50 hours [3]. For the production of parts by additive manufacturing, ball milling on machining swarf caused the formation of stainless steel powders. Length of the machining chip as starting material was between 5mm to 20mm. Used ball size changed the shape of powder and size of the powdered particles. Both the theoretical and experimental tasks were to analyse the ball milling features. Larger balls caused efficient breaking of machining chips resulting coarser particles and smaller balls changed the powder shape to spherical. Thereafter, ball milling using initial larger balls for ball milling followed by second-type ball milling by smaller balls was a better choice. Near-spherical-shaped powdered (38 μm to 150 μm) particles formed and were successfully applied in additive manufacturing for laser-engineered net shaping [4]. Austenitic stainless steel chips were balled milled to form Nano crystalline stainless steel powder. Deformation of chips during ball milling caused transformation from austenite to martensite with grain size of 15 nm. Annealed powder particles resulted transformation to austenite [5]. The ball milling of stainless steel chips along with vanadium carbides caused powdered particles. Blending, compaction, and sintering on powdered particles formed the specimen. The sintered item showed the presence of ferritic, austenitic and martensitic phases. The density and porosity were lesser [6]. Machining was for the very low carbon steel and low carbon steel. After the chip collection, cutting resulted smaller sized chips. Planetary ball milling was to form powder particles with sub- micron sizes by milling for different time. Three hours of milling time were to obtain the smallest particles for both cases. However, for very low carbon steel, cold welding and coalescence of particles occurred during milling for 5 hours. These effects declined during the milling of low carbon steel for 5 hours. Higher ball to powder ratio caused reduction of micron sized particles. 1% Yitria was added to both the steel powders. Making specimens both for yttria-free and yttria-added cases with powder was for compaction and sintering. Hardness increased significantly in both the sintered powders with yttria addition [7]. The duplex stainless steel chips (approx. mean size = 8 mm) were available. High-energy ball milling was for planetary ball milling work with vanadium carbide addition to chips. Application of response surface methodology resulted in optimal milling parameters. The process parameters were milling time, rpm, % addition of vanadium carbide, and mass/ball ratio. The addition of vanadium carbide enhanced the reduction of particle size. Theoretical and experimental results were in good agreement [8].

Experimental Procedure

The length and diameter of the round EN47 steel bar was 500 mm and 75 mm. The main cutting edge angle (ϕ) of the Miranda brazed carbide tool was 46^0.

Table 1 shows the parameters of the variable machining process.

Table 1. Experimental parameters

Expt. No.	R.P.M, [Rev./min]	Feed, F [mm/rev.]	DOC, D [mm]	Time, t, [sec]
1	400	0.1	1	5
2	400	0.1	1	10
3	400	0.1	1	15
4	630	0.1	1	5
5	630	0.1	1	10
6	630	0.1	1	15
7	1000	0.1	1	5
8	1000	0.1	1	10
9	1000	0.1	1	15

The following shows the steps of work:

(1) Variable machining, (2) Chip collection, (3) mounting of chips and Chip thickness measurement (photo software method) (4) SEM observation of chip surface (5) Tensile test for the specimen for determination of strain hardening index (n) and strength co-efficient (K).

Theory The equation 1 is the formulation for the chip reduction co-efficient (ç).

$$ç = \frac{h2}{h1} \quad (1)$$

Where, h1 is the uncut chip thickness and h2 is the formed chip thickness.

The equation (2) [9] is the formulation for the uncut chip thickness (h1).

$$h1 = So * Sin(\phi) \quad (2)$$

where So is the feed and ϕ is the main cutting edge angle.

Results and discussion

The as-received hardness of the material was 45.9 HRC.

Fig. 1 shows the machining chips for all the experimental parameters. The particulate chips are available for expt. Nos. 1, 2, 3, 4, and 5. Expt. no. 6 shows the mixture of semi-continuous, arc and particulate type of chips. Arc-type chips were available for expt. No. 7 and 8. Expt. No. 9 shows the formation of mostly semi-continuous, and arc type chips. The smallest particulates, however, formed at expt. No. 3. Studies preferred for expt. no. 3, 6, and 9 for chip formation mechanism. Fig. 2(a), (b), and (c) show the chip cross-section, scale, and chip thickness for experiment no. 3. The Fig2 (d), (e), and (f) show chip cross-section, scale, and chip thickness for experiment no. 6. The Fig2 (g) and (h) (i) show chip cross-section, scale, and chip thickness for experiment no. 9.

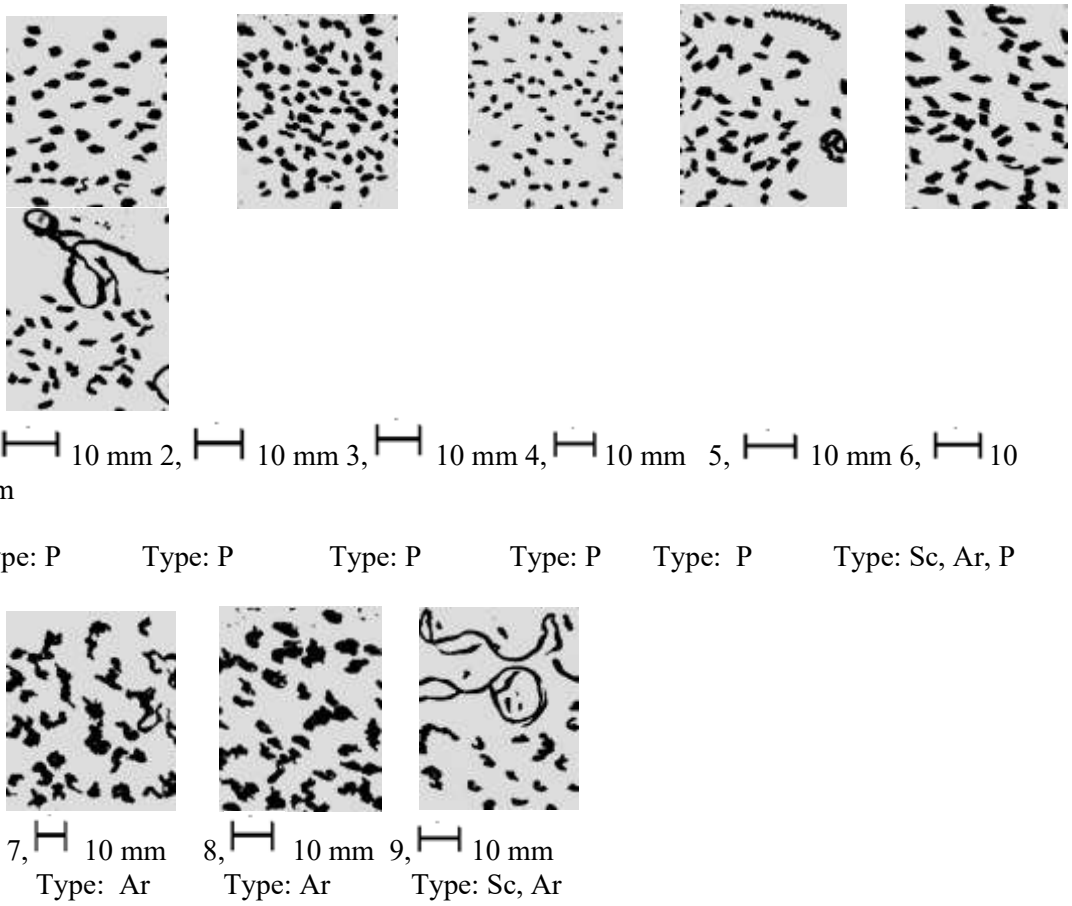

Fig. 1 Types of chips that formed during machining P: Particulate, Sc: Semi-continuous, Ar: Arc

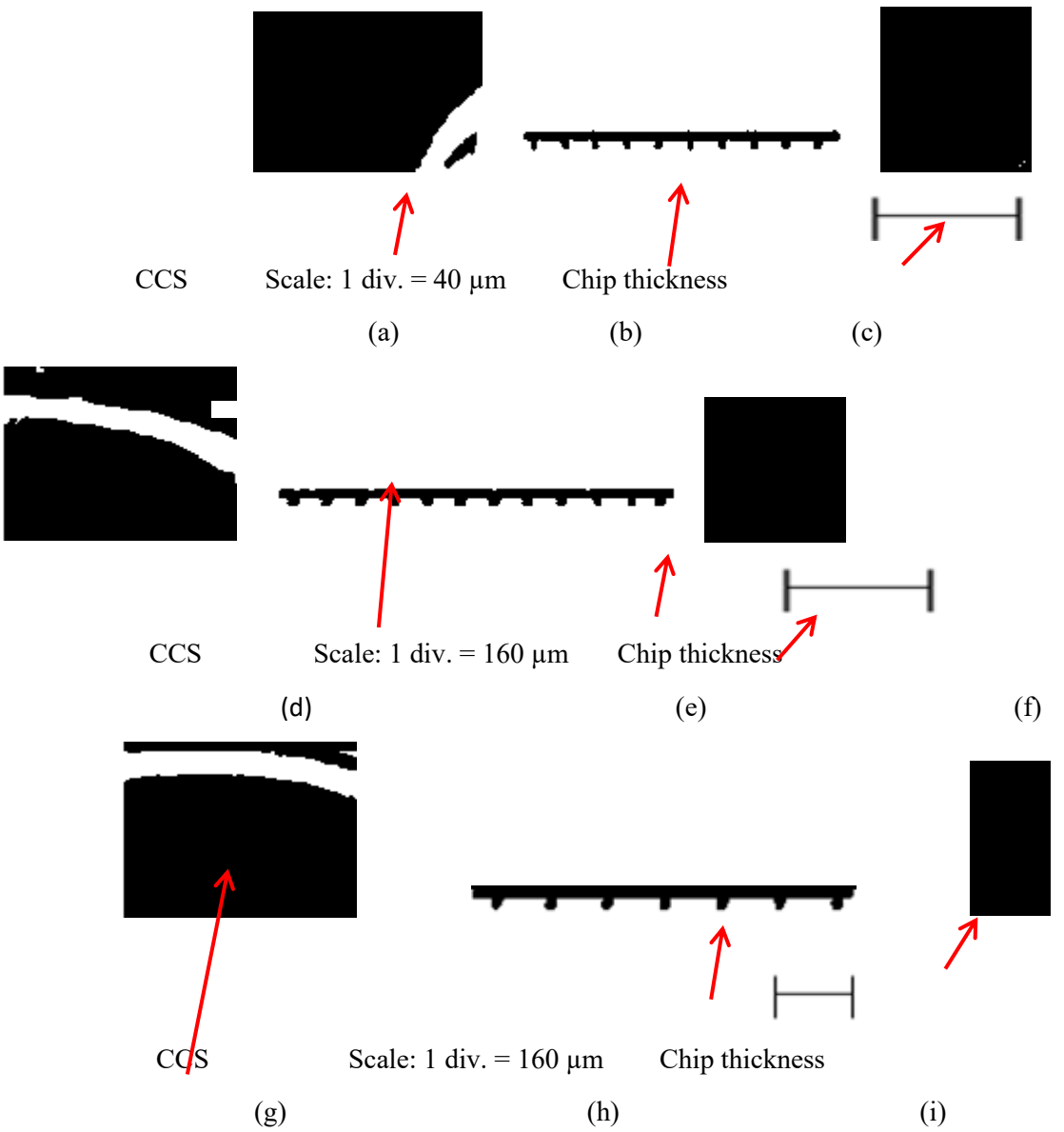

Fig. 2 For speed 400 rpm, (a) Chip cross section (CCS), (b) Scale, (c) Chip thickness; for speed 630 rpm, (d) Chip cross section (CCS), (e) Scale, (f) Chip thickness; for speed 1000 rpm, (g) Chip cross section (CCS), (h) Scale, (i) Chip thickness (F=0.1 mm/rev. D=1 mm, t=15sec)

Table 2 shows the measured chip thicknesses. Lowest chip thickness (0.18 mm) was for smallest particulate chip at 400 rpm. Size of the particles ranged between 0.8 mm to 2.5 mm (avg. size < 2mm).

Table 2. Chip thicknesses at different experimental conditions, (F = 0.1 [mm/rev.], D = 1[mm], t = 15[sec])

RPM	400	630	1000
Chip thickness (mm)	0.18	0.64	0.28

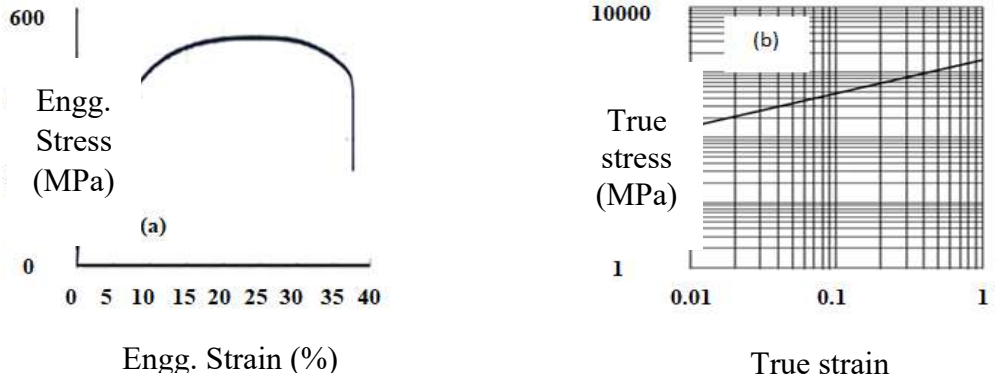

Fig. 3 (a) Engineering Stress-engineering strain graph, (b) The true stress- true strain graph (Log-Log).

The tensile test resulted in the stress-strain curve (Fig. 3(a)). Three points were considered in between the yield point and the ultimate strength point on this curve. Determination of corresponding engineering stress and engineering strain values from this graph helped to determine the true stress (σt) and true strain (ϵt) graph (Fig. 3(b)) using the equation (3) and equation (4) [11, 12].

$$\sigma t = \sigma (1 + \epsilon) \quad (3)$$

$$\epsilon t = \ln (1 + \epsilon) \quad (4)$$

Noting and joining of these three points on log-log graph paper resulted in the straight line according to Fig. 3(b). The slope of this straight line provided the strain hardening exponent 'n'. The point of intersection of this straight line with the vertical line at true strain = 1 and subsequent horizontal straight line at this point of intersection intersected the true stress axis

to provide the strength coefficient "K". The strength coefficient and strain hardening exponent were 1714.29 MPa and 0.3639, respectively. The substitution of "n" and "K" resulted in the power law equation (5) [$\sigma t = K(\epsilon t)^n$] as

$$\sigma t = 1714.29\ (\epsilon t)^{0.3639} \quad (5)$$

Finally, the equation (6) [10] provided the von Mises stresses at three experimental points.

$$\sigma v = 1.74 * K * (\ln ç)^n \quad (6)$$

Where σv is the von Mises stress.

Table 3 shows the CRC and von Mises stress.

Table 3. CRC(ç) and VMS

RPM, [Rev./min]	CRC	VMS [MPa]
400	2.5022	2890.40
630	8.8970	3964.53
1000	3.8924	3335.14

VMS increases as the speed increases from 400 rpm to 630 rpm, and again, VMS decreases as the speed increases from 630 rpm to 1000 rpm (figure 4).

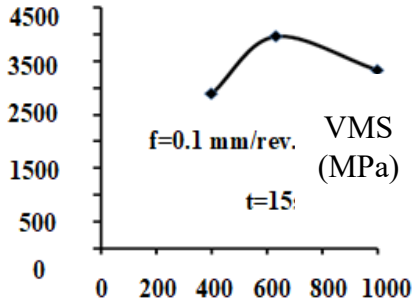

Fig. 4 Variation of VMS w.r.t RPM (F = 0.1 mm/rev., D = 1 mm, t= 15 sec)

The scanning electron microscopy study for the top surface of the chip (400 rpm) showed numerous cracks (Fig. 5a), indicating catastrophic breakage of the chip at this machining condition. This caused the lowest VMS (2890.40 MPa) generation during machining at this condition. This is attributed to the low temperature generation at lower speeds. The material strain hardens extensively, for which cracks form easily. The strain hardening index value was at a higher degree (n = 0.3639) for this material. The scanning electron microscope showed the top surface of the chip for 630 rpm (Fig. 5b). The chip showed massive ductile deformation. The side flow of the material took place extensively (Fig. 5b). These features caused higher VMS (3964.53 MPa) at this machining condition. The chip thickness at these machining parameters was also higher (0.64 mm), and that implied massive deformation in ductile mode. For 1000 rpm, the deformation of the chip however occurred by the formation of a dislocation cell, followed by the formation of an elongated sub-grain and subsequently the division of the elongated sub-grain (Fig. 5c). Fig. 6 a, b, c, and d show the mechanism of formation of subdivided elongated sub-grains. The chip formation occurred by a partial thermal effect, for which the chip thickness was moderately higher (0.28 mm). The high-speed machining resulted in moderately higher chip thickness. This resulted in a slightly lower VMS (3335.14 MPa) at this machining condition due to a partial increase in temperature.

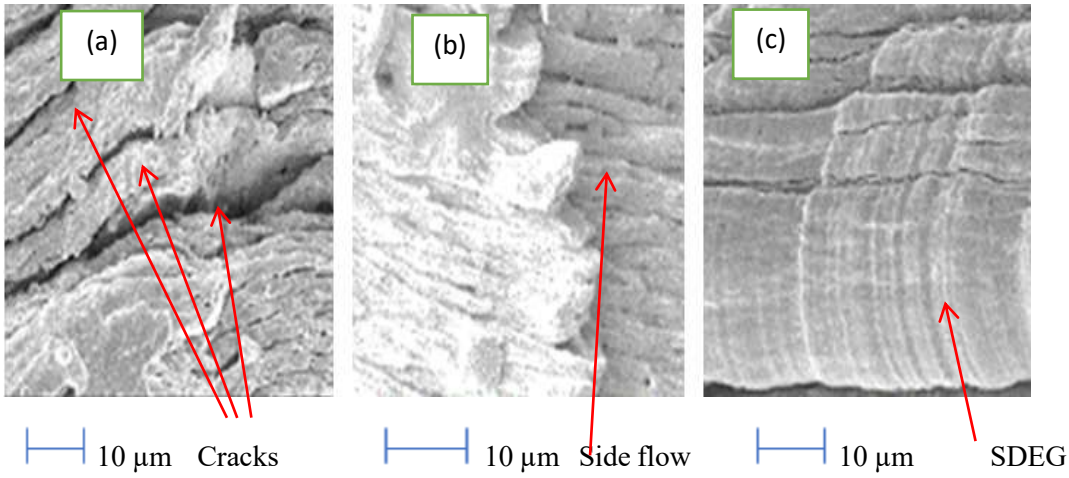

Fig. 5 (a) SEM image of the top surface of the chip, 400 rpm, (Expt no. 3), (b) SEM image of the top surface of the chip, 630rpm, (Expt. No.6), (c) SEM image of the top surface of the chip, 1000 rpm, (Expt.no.9) (SDEG: sub-divided elongated grain)

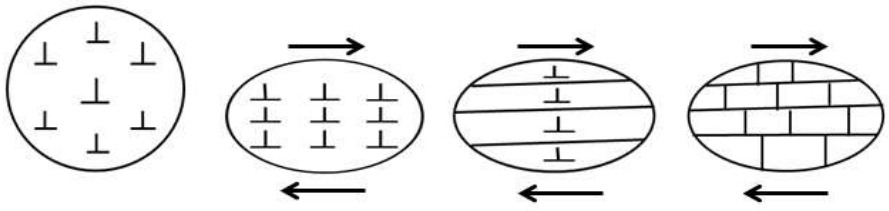

(a) (b) (c) (d)

Fig. 6 (a) Dislocation filled-up equiaxed grain, (b) dislocation cell, (c) elongated sub- grain, (d) division of elongated sub-grain.

Conclusion

It is possible to reduce the size (<2 mm) of machining chips to particulate in kind by variable machining. Thus, the prior cutting operation of chips to smaller sizes is avoidable. Moreover, milling time reduction during the ball milling operation takes place. At a specific machining condition (N = 400 rpm, F = 0.1 mm/rev., D = 1 mm, t = 15 sec), the formed chip breaks catastrophically due to extensive strain hardening, causing the formation of numerous cracks. This happens as the strain hardening index of the material was relatively higher (n=0.3639). Amount of deformation during chip formation at this condition was lowest (chip thickness = 0.18 mm). The VMS at this machining condition reduces appreciably (2890.40 MPa) due to the brittleness transition of the material.

At moderate speed (630 rpm) with similar machining conditions (F = 0.1 mm/rev., D = 1 mm, t = 15 sec), the chip formation occurred through ductile mode. Extent of deformation during chip formation was higher (chip thickness = 0.64 mm) and that caused higher VMS generation (3964.53 MPa). The chip sizes were relatively larger.

During machining at 1000 rpm under similar machining conditions (F = 0.1 mm/rev., D = 1 mm, t = 15 sec), the chip formation occurred by the formation of a dislocation cell following elongated sub-grain formation. Such elongated sub-grain got subdivided. The chip thickness under such conditions was slightly higher (0.28) due to moderately higher temperature generation. This caused moderately higher VMS (3335.14 MPa).

References

[1] H. K. Basukumar, K. V. Arun, Experimental investigation on hydrogen embrittlement of EN 47 spring steel, IOP conference series, (2021) Series: Materials Science Engineering, 1126 (2021) 012077, DOI: 10.1088/1757-899X/1126/1/012077

[2] S. Banerjee, B. Panja, S. Mitra, Study of MRR for EN 47 spring steel, in WEDM, Materials Today Proceedings, 5, (2018) 4283-4289

[3]A.N.O. Dias, M. R. D. Silva, & G. Silva, Influence of ball milling parameters on microstructure and magnetic properties of aluminum bronze chips reinforced with vanadium carbide. The International Journal of Advanced Manufacturing Technology. 115 (2021) 2205–2218. https://doi.org/10.1007/s00170-021-07250-9.

[4] B. Fullenwider, P. Kiani, J. M. Schoenung, K. Ma, Two-stage ball milling of recycled machining chips to create an alternative feedstock powder for metal additive manufacturing. Powder Technology. 342 (2019) 562–571. https://doi.org/10.1016/j.powtec.2018.10.023

[5] M.H. Enayati, M. R. Bafandeh, S. Nosohian, Ball milling of stainless steel scrap chips to produce nanocrystalline powder. J Mater Sci. 42 (2007) 2844–2848. DOI 10.1007/s10853-006-1371-2

[6] C. D. S. P. Mendonça, V. A. D. S. Ribeiro, M.M.J.D. Sachs, L. A. L. Oliveira, M. L.. N. M. Melo, G. G. Silva, Recycling Chips of Stainless Steel by High Energy Ball Milling. Materials Science Forum. Trans Tech Publications, Switzerland, ISSN: 1662-9752, 930 (2018) 454-459. doi:10.4028/www.scientific.net/MSF.930.454

[7] P. Verma, R.Saha, D. Chaira, Waste steel scrap to nanostructured powder and superior compact through powder metallurgy: Powder generation, processing and characterization. Powder Technology. 326 (2018) 159–167.

[8] F. Gatamorta, C. S. P. Mendonca, M. M. Junqueira, E.Bayraktar, B. G. Andrade, M. D. L. M., Melo,& G. Silva, Optimization of the High Energy Milling Process of Chips of a Stainless Steel Using the Response Surface Modeling. Mechanics of Composite, Hybrid and Multifunctional Materials, 5, Conference Proceedings of the Society for Experimental Mechanics Series, Springer, https://doi.org/10.1007/978-3-319-95510-0_29
[9] A. Bhattacharyya, Metal cutting. New Central Book Agency, Calcutta, 1984
[10] V. P. Astakhov, Tribology of Metal Cutting; Briscoe, B.J., Ed.; Tribology and Interface Engineering Series, No. 52, Elsevier, Amsterdam, the Netherlands, 2006.
[11] W. D. Callister, Materials science and engineering, An Introduction, Wiley
[12] Z. D. Jastrzebski, The nature and properties of engineering materials, Third edition Wiley